Photoinduced multistable resonance frequency switching of phase change microstring at room temperature

Bukhari, Syed A.; Mcgee, Ryan; Mahdavi, Amirhossein; Bensebaa, Farid; Zhou, Liang; Chung, Hyun-Joong; Thundat, Thomas; Goswami, Ankur

Publisher's version / Version de l'éditeur:
https://doi.org/10.1002/aelm.202100819
Advanced Electronic Materials, 2021-12-22

S. A. Bukhari,* R. McGee, A. Mahdavi, F. Bensebaa, L. Zhou, H.-J. Chung, T. Thundat,* A. Goswami* 2100819

Photoinduced Multistable Resonance Frequency Switching of Phase Change Microstring at Room Temperature

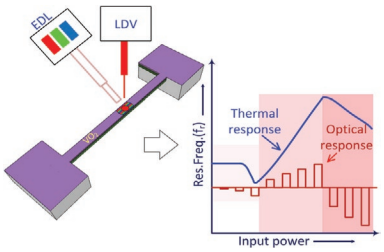

Photoinduced insulator to metal transition in phase change microstring resonator demonstrates multiple stable mechanical frequencies at room temperature at extremely small excitation power. This frequency response can also be altered by changing the wavelength of excitation laser. This work demonstrates extremely sensitive detection of phase transition, spatial control of transition volume at extremely high speeds opens the avenue for energy efficient neuromorphic platforms.

Q2

ADVANCED ELECTRONIC MATERIALS
www.advelectronicmat.de

Photoinduced Multistable Resonance Frequency Switching of Phase Change Microstring at Room Temperature

Syed A. Bukhari,* Ryan McGee, Amirhossein Mahdavi, Farid Bensebaa, Liang Zhou, Hyun-Joong Chung, Thomas Thundat,* and Ankur Goswami*

Vanadium dioxide (VO_2), a promising phase change material, exhibits insulator to metal transition at 68 °C, manifests a drastic change in multiple physical properties, such as electrical resistance, mechanical modulus, lattice parameters, etc. From technological perspective, the transition temperature can be reduced by precise strain engineering. Here a noncontact, all-optical, and highly energy efficient platform is demonstrated to study macroscopic dynamics related to the localized structural rearrangements at room temperature. A thin layer (≈25 nm) of polycrystalline VO_2 deposited on a platinum coated silicon nitride microstring resonator shows a fast controlled mechanical resonance frequency response upon variations in optical power and wavelength. It is shown multiple stable frequencies of the resonator, designated as different equilibrium states, can be activated at different optical powers (≈200 µW) and wavelength, i.e., 450, 520, and 635 nm. The observed multiple resonance states of the microstring are explained because of the generation of stress due to the interplay between thermal expansion and the temperature-induced phase change of VO_2. It is believed this change in frequency states under the controlled external optical excitation can have potential applications in ultrafast optical switching, intelligent temperature sensors, and neuromorphic devices operated at room temperature.

Resonators based on microelectro-mechanical systems (MEMS) have attracted significant attention over the past couple of decades because of their utility in bistable and multistable switches for potential applications in accelerometers,[1] microrelays,[2] logic gate,[3] actuators,[4] radio frequency switches,[5] nonvolatile memory devices,[6] neuromorphic systems,[7] etc. A resonating device is bistable, if its resonance frequency changes from an initial value to a final stable value (only one ON state) under an external trigger (e.g., photo, thermal, electric field, etc.) and returns to the original state (OFF state) upon removal of the triggering pulse. Unlike a bistable system, a tristable (or multistable) system can toggle between all the available stable states under external triggering.[8,9] A multistable resonating device can have multiple equilibrium frequency, phase, or amplitude states depending on the changes in its physical properties (stiffness, coefficient of thermal expansion, dielectric constant, etc.) induced by external stimuli. In silicon MEMS resonators, the changes in the resonance frequency usually show bistable states under heating since its mechanical modulus varies uniformly with temperature. However, by integrating a phase change material (PCM) with conventional silicon MEMS, it is possible to engineer a device with multiple stable states, with negative and positive changes in the frequency, that can be toggled by fine control of external stimuli.[10] For the bistable resonant devices reported in the literature,

S. A. Bukhari
Nanotechnology Research Centre
National Research Council of Canada
Edmonton, AB T6G 2M9, Canada
E-mail: smanzoor@ualberta.ca

S. A. Bukhari, R. McGee, H.-J. Chung, T. Thundat, A. Goswami
Department of Chemical and Materials Engineering
University of Alberta
Edmonton, AB T6G 1H9, Canada
E-mail: tgthunda@buffalo.edu; agoswami@mse.iitd.ac.in

R. McGee
Texas Instruments Dallas
TX 75243, USA

A. Mahdavi
Department of Mechanical Engineering
University of Alberta
Edmonton, AB T6G 1H9, Canada

F. Bensebaa
Mining and Environment (EME)
National Research Council of Canada
Ottawa K1A 0R6, Canada

L. Zhou
Department of Physics
University of Alberta
Edmonton, AB T6G 2E1, Canada

T. Thundat
Department of Chemical and Biological Engineering
University at Buffalo
The State University of New York
Buffalo, NY 14260, USA

A. Goswami
Department of Materials Science and Engineering
Indian Institute of Technology, Delhi
Hauz Khas, New Delhi -110016, India

The ORCID identification number(s) for the author(s) of this article can be found under https://doi.org/10.1002/aelm.202100819.

DOI: 10.1002/aelm.202100819

such as capacitive microcantilever[8] and silicon nanowire coupled with ring resonators,[11] the underlying physics is based on the force gradients, electrostatic, optical, or thermal, generated from differential thermal expansion. However, MEMS-based bistable or multistable switches that are based on phase transition of material due to external stimuli, are still remain under represented in literature except few recently.[12] By exploiting the phase change mechanism, multistable resonating systems can be realized for ultrafast optical switching, neuromorphic devices, and auto intelligent temperature sensors.[13]

Vanadium dioxide (VO_2), a canonical example of a transition metal oxide with correlated electrons, undergoes a sharp and reversible first order metal-insulator transition, known as Mott transition, at 68 °C (critical temperature, T_C).[14] When cooling through the T_C, the transition is realized as an off axis dimerization of alternating vanadium atoms along the *c*-axis of the tetragonal phase, which results in drastic changes in the electrical, optical, and structural properties of the film.[15] The T_C varies depending on the crystallinity, grain size, texture, and quality of material phases. This transition results in an ultrafast (sub-ps) change in the electrical resistance by up to four orders of magnitude, which may also show a hysteresis in the heating/cooling cycles.[15,16] The hysteresis can be significantly affected by the same variables that influence the T_C. In addition to electrical resistance, physical properties, such as elastic modulus, refractive index, heat capacity, thermal expansion coefficient, etc., may also change drastically during this phase transition.[17] A significant number of studies have been devoted to VO_2 thin films in order to optimize and control the transition temperature, the hysteresis width, and the magnitude of changes in the physical properties (especially resistance).[18] However, a controversy still persists regarding whether the electron–electron (Mott–Hubbard mechanism) or the electron-lattice (Peierls's transition) interactions is responsible for the phase transition.[19] Despite the disagreement about the underlying mechanism, significant advances have been made in the development of electronic switches,[20] smart windows,[21] optical modulators,[22] band pass filters,[23] and self-actuators [24] by exploiting this transition behavior of VO_2. A well-studied chalcogenide semiconductor $Ge_2Sb_2Te_5$ (GST) system has also demonstrated superior applications for interfacial phase change memory[25] which now became a prototype phase change system for applications in neuromorphic computing. These materials were also studied optically by tuning the refractive index of the material.[26],[27]

By leveraging the Mott transition of vanadium dioxide (VO_2) on devices under different external excitation phenomenon have been explored, but very few focused on MEMS devices.[28] For instance, Seo et al. studied the bistability by developing photoassisted electrical switches which measures voltage using two-terminal devices under illumination with infrared (IR) light.[29] Similarly, thermomechanical bistability has also been proposed theoretically in VO_2 coated silicon dioxide microcantilever by applying heat from a radiative source.[30] Further, Cao et al. reported bistability in MEMS devices by demonstrating bidirectional resonance frequency tuning using prebuckled VO_2 coated micro bridge through Joule heating mechanism.[31] Recently, bidirectional frequency tuning in VO_2 based suspended microstrings was also demonstrated by Bukhari et al. using a pump–probe technique.[10] Efforts are presently underway to develop nonvolatile programmable memory devices employing bistability in VO_2 systems by measuring resonance frequency of the free-standing device using Joule heating principle and photoinduced carrier generation.[32] Although there are a few reports on photoinduced electrical switches and photothermal actuators enabling bistability as discussed earlier, they were restricted to two-terminal devices only.[23,29] However, the required external power remains very high (50–100 mW) to activate the device because of the large thermal mass involved. In all the previous studies, prior to activating the device into bistable mode via external stimulus, the device was brought to the onset of the transition zone by placing the device on a heating stage. Multistable nature of VO_2 based MEMS devices have not been explored until now.

Recently, optical pump–probe technique was used for detecting and controlling the ultrafast (<1 ps) phase transition of VO_2 thin films by utilizing transmittance change in terahertz radiation.[33] The fact that such transition can be modulated spatially at confined distance (nm)[34] with very fast time scale (picoseconds) led us to integrate VO_2 thin films with conventional silicon MEMS. We have used suspended microstrings as resonators to probe dynamic mechanical response as a function of photoexcitation because of their extremely low thermal masses. Laser irradiation-induced temperature increase of the resonator changes its resonance frequency similar to that observed with conventional heating. This change in frequency can be attributed to interplay between the changes the elastic modulus due to solid–solid phase transition of the VO_2 and the thermal expansion of the microstring. It was assumed that the spatial control of the transition can result in multiple eigen frequencies of the resonator depending on the power or wavelength of the external excitation source. Laser irradiation of the VO_2 microstring resonators were achieved by using pump–probe technique with two different light sources. The probe was the internal light source of the Laser Doppler Vibrometer (LDV), referred to as the internal laser source (ILS) from now on, which has a wavelength of (λ_{ILS}) of 633 nm. The optical power of this internal laser of the LDV can be varied from 20 to 220 µW at power levels of 20, 30, 40, 50, 70, 120, and 220 µW as set by the manufacturer. The pump laser source was an external diode laser (EDL), consisting of three different diode lasers with wavelengths (red, λ = 635 nm, green, [illegible] nm, and blue, [illegible] nm). The power of the EDL can be set at 30, 70, or 100 µW. The temperature-induced changes in physical properties of VO_2 can enable reversible changes in the mechanical resonance frequency of the microstring. We found that there exist multiple resonance frequencies for the same eigen mode, which can be excited by changing the wavelength and the power of the EDL source. This phenomenon offers a unique opportunity to design programmable MEMS or NEMS devices to develop non-Boolean computational paradigms,[35] ultrafast switches,[36] that can be operated at room temperature using optomechanical oscillators.[37] The resonance response of the device dependents on the power of the incident light, and therefore pump–probe arrangement allows triggering phase transition in VO_2. In these experiments, we have kept the power of the probe laser (ILS) constant while pulsing the power of the EDL for triggering the phase transition. The effect of various power levels of ILS and EDL as well as different wavelengths of EDL on triggering different stable states were systematically investigated.

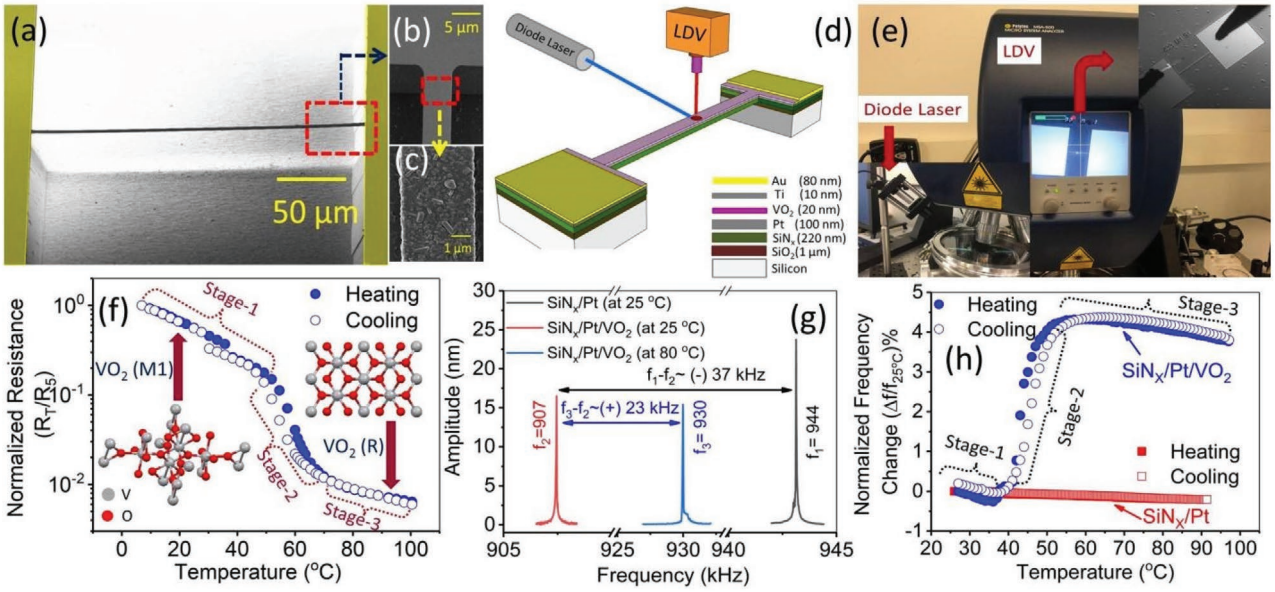

Figure 1. Fabrication and characterization of free standing $SiN_x/Pt/VO_2$ microstring. a) SEM of the suspended $SiN_x/Pt/VO_2$ microstring. b) Magnified part of the anchor point of a) shows the width of the beam. c) SEM of the selected part of b) shows the microstructure of the deposited VO_2. d) Schematic of the fabricated microstring showing the different layers it made up of, and the experimental setup containing LDV laser (ILS) and EDL for measuring and triggering the resonance frequency (f_r) respectively. e) Photograph of the experimental setup containing LDV, vacuum chamber and EDL. Inset shows two microprobe pins probe the suspended microstring. f) Resistance versus temperature plot of the $SiN_x/Pt/VO_2$ microstring showing three stages of the resistance change. Both monoclinic (M1) and tetragonal crystal structure of VO_2 are shown at stage-1 and stage-2, respectively. g) Frequency versus amplitude plot of SiN_x/Pt and SiN_x/Pt /VO_2 microstring at 25 °C and $SiN_x/Pt/VO_2$ microstring at 80 °C. The first eigen mode of f_r of the microstring is shown. The ILS power was kept 20 µW in all the cases. h) Shows change in f_r with function of temperature for SiN_x/Pt /VO_2 and SiN_x/Pt microstring.

Figure 1 depicts a microstring resonator fabricated from suspended silicon nitride (SiN_x), coated with 100 nm of Pt and 20 nm of VO_2, respectively. Figure 1a–c shows SEM images of the microstring and the microstructure of the deposited VO_2. Structural characterization of VO_2 was performed by XRD and Raman spectroscopy as described[15,38] (also shown in Figure S1 in the Supporting Information). Figure 1d shows the schematic of the experimental setup for monitoring the resonance frequency of the microstring device using LDV. The device was mounted on a peltier heater attached to a heat sink (copper block) in order to heat the device conventionally. A piezoelectric actuator and a Pt-1000 temperature sensor were placed on the chip containing the device in order to actuate the microstring into resonance and to measure the temperature, respectively. The whole setup was kept inside a vacuum chamber at 1×10^{-6} torr, while performing the measurements. Details of fabrication process of these microstrings are shown in Figure S1 (see the Supporting Information). The photograph of the whole setup is shown in Figure 1e which consists of the LDV and the vacuum chamber with an EDL (see bottom inset Figure 1e). Schematic of the setup is shown in Figure S2 (see the Supporting Information). An image of the two-probe measurement of the microstring straddling two terminal pads is shown in top inset Figure 1e. The Peltier element was also used for controlling the temperature of the microstring during the resistance measurements with a Keithley 197a multimeter. Normalized resistance of the microstring as a function of temperature is shown in Figure 1f. During heating, the resistance of the microstring changes nearly three orders of magnitude as the VO_2 undergoes metal-to-insulator (monoclinic, M1, to rutile, R) transition. As expected, this transformation is reversible and shows negligible hysteresis due to the small grains of the deposited VO_2 layer as also observed in the earlier work.[39] The resistance versus temperature curve, shown in Figure 1f, displays a sharp reduction in the electrical resistance, which indicates the insulator-metal phase transition of VO_2 on the microstring.

The resonance frequency (f_r, the first eigen mode) of the microstring was measured using LDV as shown in Figure 1g. While measuring the f_r of the microstring, the ILS power was fixed at its lowest value of 20 µW in order to minimize laser-induced heating of the microstring. The control microstring fabricated with only SiN_x/Pt had a resonance frequency, f_r, of 944 kHz. After deposition of VO_2 on the microstring (SiN_x/Pt), the f_r was found to be 907 kHz at 25 °C, a decrease of 37 kHz due to mass loading. However, an increase in the device temperature from 25 to 80 °C caused an increase of 2.5% in the f_r (from 907 to 930 kHz), which can be attributed to a combined effect of increased stiffness and tensile stress (as per Equation (S1), Supporting Information) of the resonator due to structral reordering-induced lattice compression in the VO_2 film. Figure 1g shows a clear difference between the two resonators consisting of SiN_x/Pt and $SiN_x/Pt/VO_2$. The former, having no MIT due to the lack of VO_2 layer, shows a negligible decrease in the f_r as a function of temperature, whereas the latter shows three stages of the f_r which resembles that of the resistance variation shown in Figure 1f. Stage-1 shows a steady decrease of the f_r due to changes in the material properties and the moment of inertia of the microstring.[40] Stage-2 shows a sharp increase in the f_r due to the MIT which adds additional tensile stress to the system

Table 1. Optical power considerations for FEM calculations.

Case-1: ILS only (single pump–probe)		Case-2: ILS and EDL pump with EDL probe with ILS			
Layers considered	Optical power-ILS [μW]	EDL = 0 [μW] ILS [μW]	EDL = 30 [μW] ILS [μW]	EDL = 70 [μW] ILS [μW]	EDL = 100 [μW] ILS [μW]
$SiN_x/Pt^{a)}$ $SiN_x/Pt/VO_2^{b)}$	20	20	20	20	20
	30	30	30	30	30
	40	40	40	40	40
	50	50	50	50	50
	70	70	70	70	70
	120	120	120	120	120
	200	200	200	200	200

a)Two layer model with Pt coated on SiN_x; b)Three layer model with VO_2 coated on Pt which is coated on SiN_x.

as explained in our earlier work.[41,42] Further increase in the temperature beyond the MIT results in a slow decrease in the f_r, which is designated as stage-3. The reduction in the f_r after the MIT is purely due to the softening of the material (decrease of elastic modulus) as a function of temperature. After completion of structural transformation of the VO_2 film, any further addition of heat will likely heat up the underlying layers of Pt and SiN_x leading to an overall reduction in the modulus of the system, and thus a decrease in the stiffness and the resonance frequency (f_r). The whole process is completely reversible with a hysteresis in the heating-cooling cycle as shown in Figure 1h.

From Figure 1, and also from our earlier work, it is clear that the resonance frequency of the VO_2 coated microstring shows unique characteristics as a function of temperature that can be attributed solely to its MIT behavior. We have also found that bidirectional variation of the f_r of the microstring (either an increase or decrease in the resonance frequency) can also be observed by changing the power of the laser, ILS.[10] Therefore, by controlling the power of the pump and probe it is possible to mouldate the f_r of the microstring without supplying any conductive heat from an exernal source, such as a peltier heater (Figure 1d). In the following section, we will describe how the power and the wavelength of the EDL, along with the power of the ILS affects the dynamics of the f_r of the VO_2 coated microstring. In this study, the ILS was used as the probe while the EDL was used as a pump for toggling the resonance frequency between multiple stable ON and OFF states of the microstring. However, it should be noted that the power of the ILS also influences the f_r by shifting the baseline frequency.

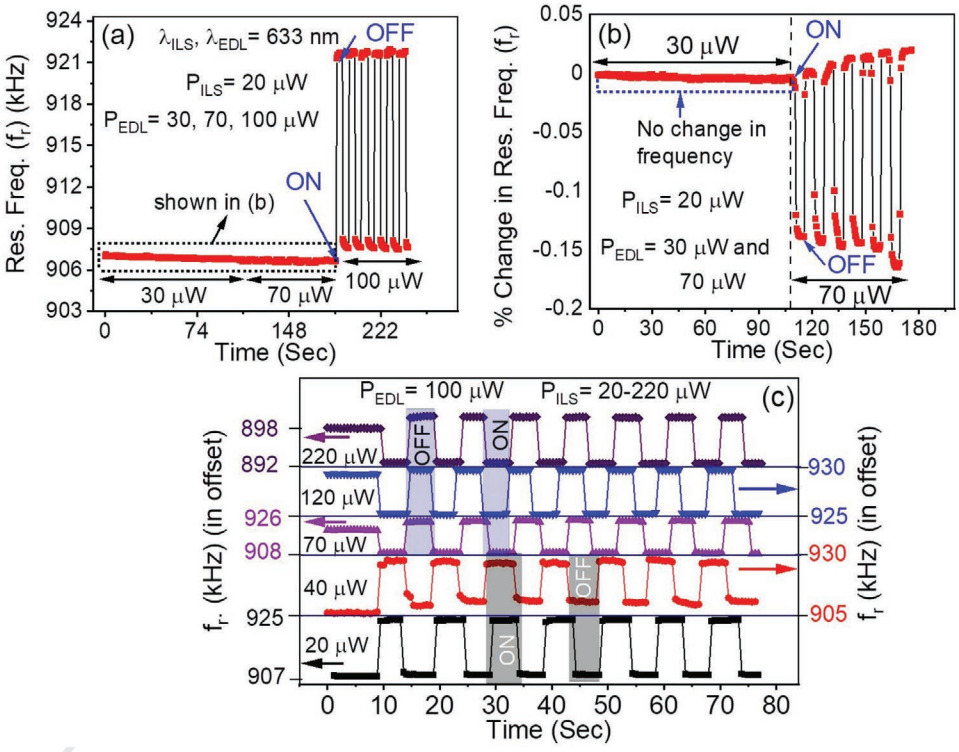

Figure 2. Multistable frequency response for 635 nm Laser. Demonstration of multistable resonance frequency (f_r) states of VO_2 microstring with different ILS and red EDL nm)power a) f_r response of microstring with ILS power of 20 μW and EDL power of 30, 70, and 100 μW. b) Magnified f_r response due to EDL power of 30 and 70 μW of a). c) Multistable frequency states at a fixed EDL power of 100 μW and varying ILS power from 20 to 220 μW. A decrease in f_r observed for ILS power ≥ 70 μW at constant red EDL power of 100 μW.

VO_2 shows a wavelength dependent ultrafast change in optical absorption below and above the phase transition in both bulk and thin films.[43] Depending on the wavelength, VO_2 film on the microstring can absorb impinging light and increase its temperature. Also, the reflective nature of Pt under layer may reflect the light back into the VO_2 causing further heating. In order to exploit the absorption behavior of VO_2 for investigating the multistability of VO_2 coated microstring resonators, it was irradiated with three different wavelengths of light (i.e., green, red, and blue) while maintaining ILS power constant (**Table 1**).

In these experiments, multistable frequency responses of VO_2 coated microstrings was studied by monitoring its resonance continuously while pulsing the laser ON and OFF (toggling) at different power. **Figure 2** shows variation of the f_r of a microstring as a function of varying the power of both the EDL ($\lambda = 635$ nm) and the ILS. Figure 2a depicts the variation in the f_r of the microstring for the three distinct power levels of the EDL while keeping the ILS power fixed at the lowest value (20 µW). Initially, the power of the EDL was fixed at 30 µW, then increased to 70 µW followed by further increase to the highest power of 100 µW. The f_r of the device was monitored as the EDL was pulsed on and off, at various power values. There are two different zones of f_r variation which are identified in Figure 2a. For instance EDL pulsing at 30 µW, no detectable changes in the f_r were measured. However, when the EDL power was increased to 70 µW, there was a subtle variation in the f_r of the microstring by 0.15% to 0.18% as shown in Figure 2b. Therefore, by turning the EDL pulse ON and OFF by using a function generator, the f_r of the microstring can be toggled from the original to the lower value. Upon further increase in the EDL power to 100 µW, a large increase in the f_r of the microstring was observed (≈1.5%) contrary to the response for the case of 70 µW. It must be noted that the changes in the f_r of the microstring were instantaneous which was beyond the limit of detection of the frequency counter used in this study (Agilent 53181A, was capable of detecting two events with a resolution of 5 ns).

Figure 2c shows the f_r variation of the microstring while toggling (ON and OFF) the EDL (from power 0 to100 µW) at 5 s intervals. During each of the measurements, the ILS was fixed at different available power levels (20, 40, 70, 120, and 220 µW) as indicated in each row of the figure and EDL was varied from 0 to 100 µW with the function of time at the interval of 5 s. During pulsing, f_r of the microstring increased instantaneously (ON state) by 1.5% and 2.5% for 20 and 40 µW, respectively, from its initial value (OFF state). However, as the ILS power was increased, the f_r was decreased, showing a decrease in the base line resonance frequency. The f_r of the microstring was in the range of 905–907 kHz for 20 and 40 µW of ILS power when EDL was off. When the ILS was increased to 70, 120, and 220 µW the overall base line of f_r shifted to 925, 921, and 887 kHz, respectively.

A VO_2 coated microstring shows a different response when pulsed with a green EDL ($\lambda = 520$ nm) at 100 µW power (**Figure 3**), than the one observed when pulsed with red EDL ($\lambda = 635$ nm)

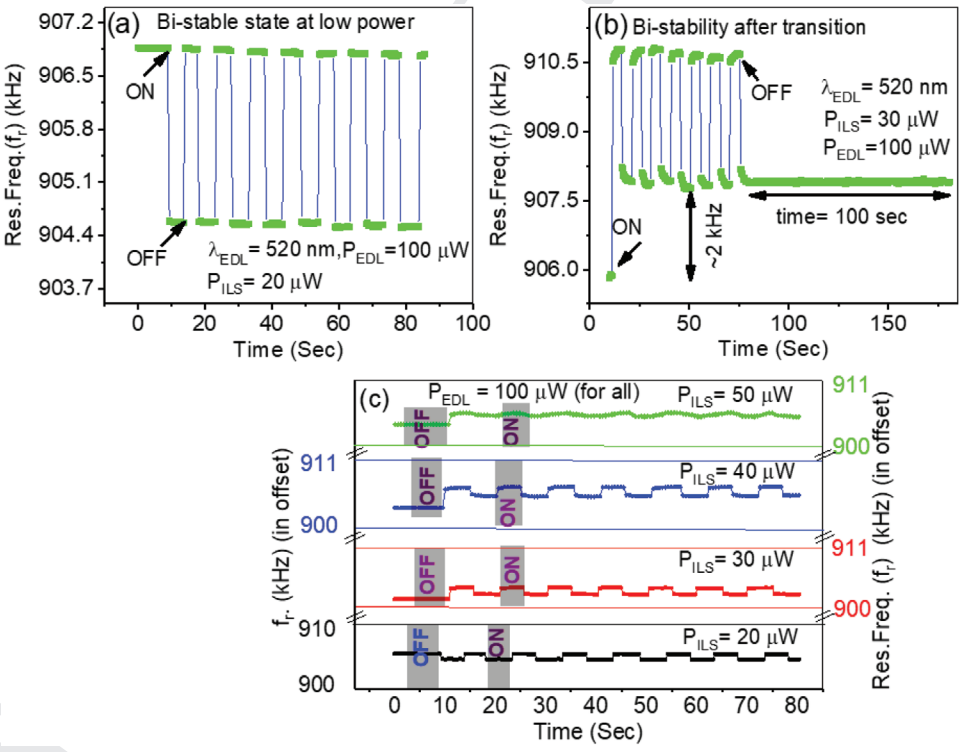

Figure 3. Multistable mechanical resonance frequencies switching of VO_2 resonator using green EDL ($\lambda_{EDL} = 520$ nm). a) Shows the bistable frequency response where exposure to EDL (at 100 µW) reduces the f_r to a stable frequency state while keeping the ILS power at minimum level of 20 µW. b) At slightly higher ILS power (i.e., 30 µW) but same EDL power, the f_r flipped to higher frequency stable state. An offset of ≈2 kHz was seen when the light was turned ON, whereas a 3 kHz frequency difference was seen between bistable states during subsequent ON/OFF cycles. Note the offset remains constant after 100 s of turning off the green EDL. In c), the ILS power was raised to 40 and 50 µW which lead to higher offset values of frequencies (≈4 kHz for 40 µW and 6 kHz for 50 µW) when the light was switched ON. However the subsequent change in frequencies during ON/OFF cycles decreased with increased optical power.

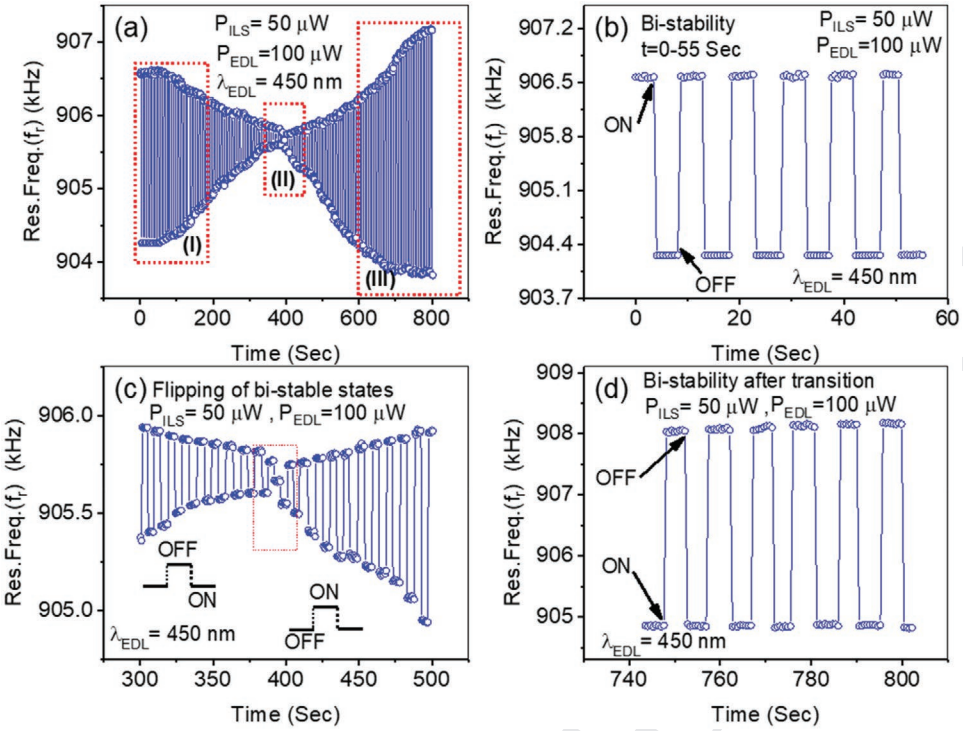

Figure 4. Time dependent switching of multistability with blue EDL (λ_{EDL} = 450 nm). Time dependent resonance frequency (f_r) response showing a transition from high-low to low-high frequency response at ILS power of 50 μW and EDL power of 100 μW. a) Three different regime of change of f_r response with the function of time was observed. b) Magnified plot of region-I where f_r changes the original state to a lower state, by a 2 kHz decrease. c) Magnified plot of region-II where it shows after 60 s of toggling of blue EDL, a decrease in magnitude of f_r was observed however the flipping of states occurred after 400 s of EDL exposure where increase in f_r was seen. d) Magnified plot of region-II where magnitude of increase in f_r of 3.5 kHz upon exposure of EDL was observed between 740 and 800 s.

(Figure 2). Here also we found a bistable resonant behavior with a drop of 3 kHz as shown in Figure 3a when the green EDL was toggled ON and OFF (0–100 μW). It should be noted that in all these cases (either in Figures 2 or 3), the probe laser, ILS, was always ON in order to measure the frequency of the microstring (20 μW). The decrease in the frequency in the case of the green EDL (Figure 3a) was an order of magnitude lower than the one obtained with red EDL (Figure 2c), though the power remained constant at 100 μW for both cases. However, it is also important to note that in both cases (either Figures 2a or 3a) the power of the ILS was set at the minimum level of 20 μW. Remarkably, when the power of the ILS was increased to 30 μW (in Figure 3b), the f_r was found to increase similar way as was observed for 100 μW power of red EDL (as shown in Figure 2b). Additionally during the ON and OFF cycles of the green EDL, the f_r of the microstring did not return to its original value of ≈906 kHz, but rather toggled between 908 and 910.5 kHz (a baseline shift of 2kHz). This offset remained stable for 100 s when EDL was turned off.

Since the absorbance of red light (635 nm) higher than the green light for VO_2 (M1) insulating phase,[44] a relatively smaller fraction of the latter is absorbed by the VO_2 film and may cause localized heating which changes the stiffness, coefficient of thermal expansion (COE), and thereby change in the f_r of the resonator. The increase/decrease in the f_r upon exposure to red/green EDL having same optical power density indicates a wavelength dependent modulation in the phase transition.[45] Because of the difference in the absorbance of the red and green wavelengths, the absorbed fraction for this power level may not be enough to heat VO_2 layer to transform it completely into the metallic state in the case of green EDL when ILS power was 20 μW. Nevertheless, an increase in f_r was observed due to EDL toggling (between 0 and 100 μW) only if the ILS power was raised from 20 to 30 μW which happens due to the localized predominantly caused by the ILS. However, the increase in the f_r is much smaller compared to the previous case where both pump and probe lasers were 635 nm. This suggests that small area exposure with the ILS can cause a small volume to transform to metallic state and thus a slight increase in frequency (≈2 kHz). This observation shows that even a small area exposure of optical power (ILS≥ 30 μW) is enough to flip bistable frequency states. Above the transition regime of VO_2 where it converts to metallic, the electronic contribution to thermal conductivity is much smaller which should not be the case for an ideal metal as predicted by Weidman–Franz law.[46] Any further increase in the optical power of ILS will likely to trap the heat within a metallic region resulting as an offset of ≈2 kHz. Further increasing the ILS power (30–50 μW), while toggling the green EDL at the same power (at 100 μW) the frequency of the device will increase under irradiation of the EDL, while it will decrease with higher offset (>2 kHz) when the EDL was turned off. At ILS power of 50 μW or beyond the change in frequency during ON/OFF cycles of EDL became very small.

To further understand the wavelength dependence of multistable response, the resonator was exposed to a blue EDL

(λ = 450 nm) with an optical power of 100 μW. Here, we again observed a bistable resonant behavior that showed a decrease in the f_r by 2 kHz when the EDL was toggled at 100 μW power. We observed similar behavior for ILS power of 20, 30, and 40 μW (data not shown). We conducted a time dependent study where we kept the ILS on at 50 μW and toggled the EDL at 100 μW, while recording the f_r as a function of time. We observed a time-dependent switching of two bistable states as shown in **Figure 4**a. Since the cross sectional area of the resonator is very small and the absorption of blue light (450 nm) is small[47] compared to red (635 nm) and green (520 nm) wavelengths, the absorbed fraction may not be enough to heat the irradiated area. This might explain why the localized transition of VO_2 was not seen in this case while toggling the blue EDL even the ILS power was enhanced till 50 μW. The frequency response of the resonator can be divided into three regions in Figure 4a. Region (I) shows a decrease in frequency upon exposure until 400 s. The magnitude of the change in frequency was found to decrease over time. The change in frequency was ≈2.5 kHz at the start of the ON/OFF cycles which then decreased to less than 0.5 kHz at 400 s. The decrease in frequency upon exposure manifests in the decrease in stiffness of the material with increase in the temperature as shown in Figure 4b. This was also observed in the previous two cases at lower ILS exposures shown in Figures 2b and 3a. The magnitude of the change in frequency upon ON/OFF cycles of the blue EDL becomes smaller as time increases. This decrease in magnitude of frequency change is likely because of a dominance of elastic modulus decrease (insulating state) as compared to the stiffness increase (metallic state) due to the time dependent phase transition within the exposed area. It is interesting to note that a sudden flip in the resonator response was observed at 400 s (region II) as shown in Figure 4c. Subsequently, the resonator showed an opposite response for ON/OFF cycles of external exposure. The magnitude of increase in frequency upon exposure was found to increase gradually over time. This increase in frequency in region III is also shown explicitly in Figure 4d. A significant fraction of light was absorbed by the VO_2 layer at this time which caused a decrease in stiffness over time as heat was trapped within a small region because of unchanged thermal conductivity leading to a decrease in modulus initially until 400 s.[48] However, upon exposing the surface for sufficient time, a net addition of heat in the resonator can trigger the localized transition higher than 400 s. A sudden change in bistability behavior dictates the onset of portion of the exposed area from insulating to metallic state leading to a stiffness increase due to the developed stress upon exposure. The magnitude of the frequency change becomes large for EDL ON/OFF cycles above 400 s as shown in Figure 4d.

From all the above three figures, i.e., from Figures 2–4 it is observed the dynamic range of tuning the frequency can vary

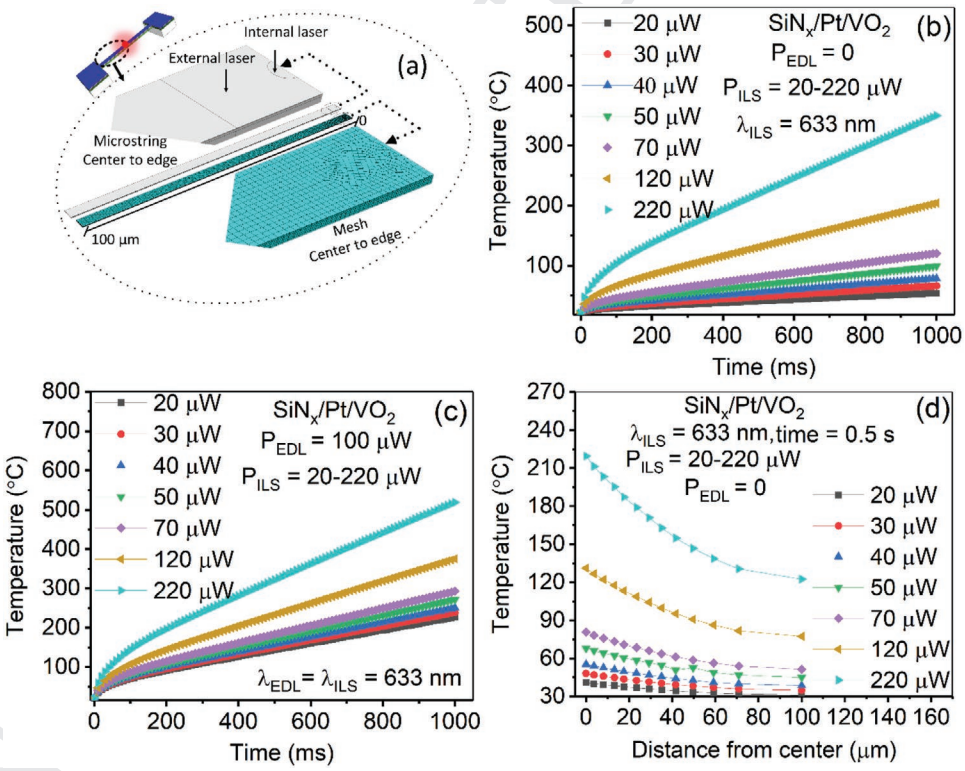

Figure 5. Finite element analysis to model transient response of microstring under the illumination of varying ILS and EDL power. a) Finite element modeling of temperature variations of VO_2 microstring at the center of the exposed area as a function of optical power and the distance from the center of the string to the edge. A generalized 3D transient heat conduction model was employed over a half of the length in order to reduce numerical cost. Exposed area by EDL was modeled as a square at the center, while the ILS was modeled as a circle with a diameter of 1 μm as shown in a). b) Time dependent temperature rise of VO_2 coated microstring at the center of the exposed area as a function of increasing ILS power only shown in c). Temperature rise of the same microstring with 635 nm EDL at exposed power of 100 μW shown in d). Transient response of VO_2 coated microstring at different optical power from the center to the edge with individual power exposed for 0.5 ms.

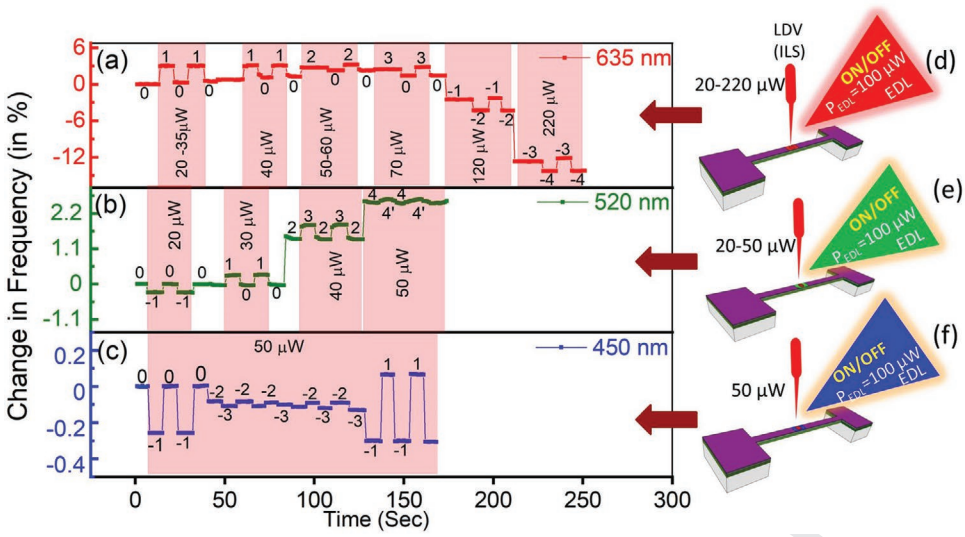

Figure 6. Comparison of change in resonance frequency (in %) of the $SiN_x/Pt/VO_2$ microstring with the function of time at different ILS power, keeping EDL power constant but constantly toggling (ON/OFF) at certain time interval during the measurement. a–c) shows the variation of the f_r state, while toggling the red, green, and blue EDL. d–f) shows the schematic of the measurement corresponding to the different EDL wavelength. In all the measurements, as shown in a–c), ILS power has been varied during the measurement which activates different frequency states. 0 corresponds to the base frequency state in all the cases, while measurements were done at 20 μW ILS power. As the ILS power increases for the measurement for different wavelength of EDL resonator respond differently. While designating the state positive integers represents increase in frequency from its base value whereas, negative integers represent the reduction in frequency from its base value.

from 0.2% to 2.7% in the proposed structure of the microstring under different illumination of wavelength and power. This range can be of course enhanced by increasing optical power or by reducing the device size which ensures lower thermal mass. Further, in all the cases the exposure of different wavelength or power of laser alters the electronic and structural characteristics of the VO_2 system which shows these variations in frequency of the resonator. However, we believe the external stimulus (in this case photon energy) does not influence the microstructure of the sample although it demands a detail study to comment anything concrete.

Since the areas exposed with the ILS (0.5 μm^2) and the EDL (1 μm^2) are very small, measurement of local temperature rise is challenging. A transient 3D heat conduction model was employed in order to estimate the temperature increase due to irradiation of light with the EDL and the ILS. Actual dimensions of the microstring were used in the calculations. Due to the symmetrical nature of the geometry and laser exposure, half length (i.e., 100 μm lengths) of the microstring was considered in the numerical modeling to reduce the computational expense (as shown in **Figure 5**a). The details of the model are explained in Figures S6 and S7 (Supporting Information). Figure 5b,c shows the variation of temperature of the microstring at two different red EDL power with the function of time at varying ILS power. It is observed that maximum temperature of the microstring can be obtained at the central area of ≈1 μm^2 under maximum power of red EDL and ILS is around 500 °C (as shown in Figure 5c. However, this is not the overall temperature of the microstring. The distribution of the overall temperature is shown in Figure 5d.

By exploiting photoinduced insulator-to-metal transition, we demonstrated the first ever reported frequency tuning with optical power nearly 200 μW. The noncontact method for probing the mechanical frequency modulation of VO_2 resonator

Table 2. Available frequency states at different EDL and ILS power.

λ_{EDL} = 635 nm, P_{EDL} = 100 μW[a)]							
P_{ILS} [μW]	20	30	40	50	70	120	200
States observed (OFF/ON)	(0, 1)	(0,1)	(0,1)	(0,2)	(0,3)	(−1, −2)	(−3, −4)
λ_{EDL} = 520 nm, P_{EDL} = 100 μW[a)]							
P_{ILS} [μW]	20	30	40	50			
States observed (OF/ON)	(0, −1)	(0,1)	(2,3)	(4,4′)			
λ_{EDL} = 450 nm, P_{EDL} = 100 μW[a)]							
P_{ILS} [μW]	50						
Time dependent Flipping of states (OFF/ON)	(0, −1)	(−2, −3)	(−3, −2)	(−1,1)			
	Flipping of states						

[a)] λ_{ILS} = 633 nm.

was achieved with a highly focused laser beam while performing the experiment at room temperature. By and large multistable resonant behavior was observed for all the EDL wavelengths. In order to compare the resonance frequency (f_r) states (multistability) for different EDL wavelenghths (and at same power of EDL, P_{EDL} = 100 µW) and different power of ILS, we summarized the results in **Figure 6**. Figure 6a shows the changes in the frequency (Δf_r in %) at different ILS power (20, 30, 40, 70, 120, and 220 µWs) while toggling the EDL (red, λ = 635 nm). Figure 6b,c represents the similar behavior of the same device using the two different EDLs (i.e., green, λ = 520 nm and blue, λ = 450 nm) at different ILS power. In Figure 6b for the green EDL, ILS power was varied 20, 30, 40, and 50 µW whereas, in Figure 6c, while using blue EDL, the ILS power was kept constant 50 µW. In all the cases 0 state represents the base f_r. If f_r increases upon irradiation with the EDL, the state is represented by positive integer and if it decreases, the state is represented by negative integer. By modulating ILS and EDL power one can tune the frequency states of microstring as shown in Figure 6. The details and designation of the states are explained in **Table 2**.

Multistable resonance frequency response as a function of temperature and optical power is depicted in a cartoon in **Figure 7**. The blue curve shows the resonance frequency of the microstring as a function of temperature obtained with conventional heating (see data shown in Figure 1h). The resonance response shows three distinct slopes (states) with two major inflection points. Heating the microstring using lasers was accomplished by keeping the ILS at constant power while pulsing the EDL. Increasing the ILS power increases the

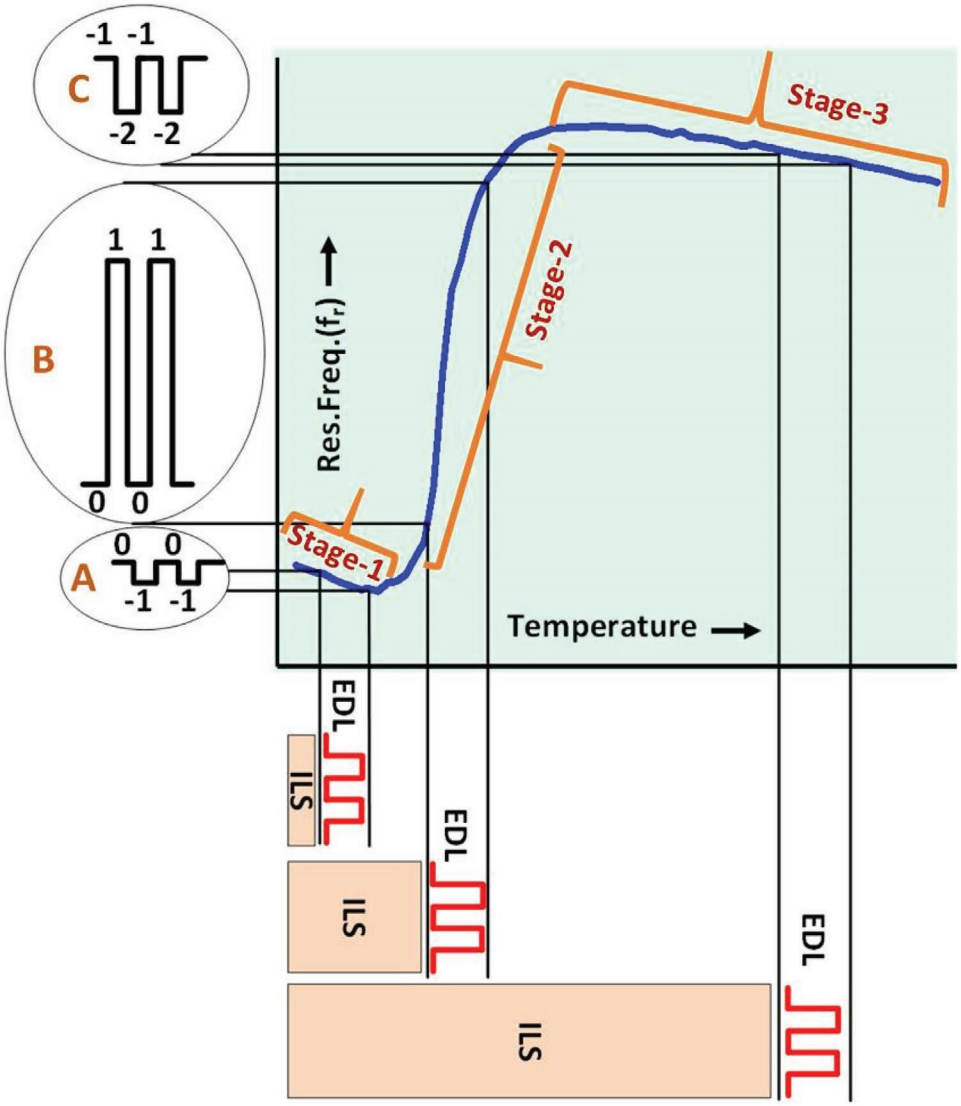

Figure 7. A schematic representation of heating of microstring resonator with relation of three distinct stages to optical power (EDL and ILS). At low ILS (20 µW) and pulsed EDL (30–70 µW), optically activated stable frequency states can be correlated with the first stage of thermal heating of the resonator. When EDL was pulsed at 100 µW, an increased frequency response upon exposure is associated with the transition stage. This is also true in case ILS is increased up to 50 µW. At higher ILS powers, the optical response is related with stage –3 of the thermal response as frequency was found to decrease upon EDL exposure.

temperature of the microstring thereby shows all three states in the resonance response depending on which power one can do the measurement. On the other hand pulsing the EDL provide extra leverage to control the frequency flipping. For instance when ILS and EDL power operates in stage-1, the frequency response of the string should be of the similar figure shown in inset-A. Similary, if both operates at the power where stage-2 and stage-3 activated then frequency response should be of the inset B and C type, respectively. However, at same power of ILS and EDL gradual flipping of the response observed in the case of the blue laser, as shown in Figure 4d, due to a time dependent heating of the microstring which allows the resonance response to travel through the inflection point of stage-1 and 2.

Depending on the wavelength of EDL, and power of both ILS and EDL, the time scale of operation or in other words stability can vary. For instance, the resonance state of the microstring is found to be stable mostly (as shown in Figures 2 and 3) at a given illumination power with the function of time for the case of red and green laser. Whereas, in the case of blue light the resonance state of the microstring varies with time at a given power of ILS and EDL. This obviously limits the potential application where long-term stability is required. As per Figure 4, the stability of the resonator toward can be observed till 50 s where downward shifting occurs. However, after 50 s, magnitude of frequency shift reduces. But if the power of illumination or time of exposure can be increased, the magnitude of the upward shift will be also stable for the same wavelength (blue) light which can circumvent the limitation.

The multiple stable states as shown in Figure 6 is due to the presence of multiple localized curvatures in the resonance response due to a combined effect of thermal expansion and localized material phase transitions.

This study does not involve any metallic interconnnects and demonstrates fast, reliable, and repeatable thermo-optical fast switching states (in all the wavelengths), memory states (in the case of 520 nm wavelength) and processing. Manipulation of mechanical frequency without any electronic ciruitry with a few hundreds of µWs of optical power may also open up avenues for auto intelligent temparature sensors with drastic reduction in energy consumption. The future direction from this study is to implement optical logic functions into phase change MEMS in the same way as implemented for microclectronics processors.

Experimental Section

Microfabrication of the suspended microstring resonators was carried out using top down lithographic technique. The fabrication process is discussed in detail in Section S1 of the Supporting Information and also in the previous work.[42] LDV, MSA Polytec 500 was used to measure the dynamic mechanical response of the resonators. The vacuum was kept 10^{-4} to 10^{-5} torr, while carrying out the measurement using LDV in order to get better Q-factor of the device. Three different EDLs from Thorlab were used (model numbers are CPS635, CPS520, and CPS450 which corresponds to 635, 520, and 450 nm wavelength, respectively) in these experiments. The power of the EDL was calibrated using a power meter (PM 100D) anticipating there would be substantial power loss, while the rays passed through the top port glass of the vacuum chamber.

Crystal structure VO_2 was confirmed using X-ray diffraction using thin film stage on Rigaku Ultima IV spectrometer as shown in Figure S5a (Supporting Information). Surface morphology of VO_2 thin films were carried out with atomic force microscope, in Figure S4b (Supporting Information).

The heat transfer due to localized heating of the microstring by the laser was modeled by using a 3D FEM technique. The FEM was developed by employing a generalized finite element solver (ABAQUS ver. 6.13, Dassault Systems Americas Corp., Waltham, MA).[49] Actual dimensions of microstring were used in calculations. In order to understand the effect of thermal conduction from the center to the edge of the microstring, the microstring was divided into 20 equal segments each separated by a distance of 10 µm. The temperature rise of the microstring from the center ($x = 0$) to the edge ($x = 100$ µm) was simulated for an exposure at the center with time duration of 0.5 ms. In case of the three-layer $SiN_x/Pt/VO_2$ resonator, the rise in temperature at the center is significantly higher (i.e., 200 °C) as compared to the edge (105 °C) for an optical power of 200 µW, as shown in Figure 5d. This large increase in the temperature along with a large temperature gradient shows the heat conduction through and along the string is anomalously lower than the two-layer system (results for two layer systems are shown in the Supporting Information). Because of small diffusivity of VO_2, heat conduction is very small which might have resulted as an increase of temperature at the exposure point and high gradient in temperature along the resonator.

Supporting Information

Supporting Information is available from the Wiley Online Library or from the author.

Acknowledgements

This work was mainly supported by the Canada Excellence Research Chair (CERC) Program (ID: SF0926 and Grant No. RES 0006296) and partly supported by IIT Delhi seed Grant No. (PLN12/04MS).The authors acknowledge the microfabrication and characterization facilities provided by the Nanofab at the University of Alberta. Rosmi Abraham and Dr. Faheem Khan are also gratefully acknowledged for useful discussions.

Conflict of Interest

The authors declare no conflict of interest.

Data Availability Statement

Research data are not shared.

Keywords

microstring resonator, phase change MEMS, Vanadium dioxide

Received: August 10, 2021
Revised: October 26, 2021
Published online:

[1] A. Holsteen, I. S. Kim, L. J. Lauhon, *Nano Lett.* **2014**, *14*, 1898.
[2] E. A. Casu, N. Oliva, M. Cavalieri, A. A. Müller, A. Fumarola, W. A. Vitale, A. Krammer, A. SchüLer, M. FernáNdez-BolañOs, A. M. Ionescu, J IEEE, *Electron Devices Soc.* **2018**, *6*, 965.

[3] A. Hamed, S. Ndao, *Sci. Rep.* **2020**, *10*, 2437.
[4] R. Shi, X. Cai, W. Wang, J. Wang, D. Kong, N. Cai, P. Chen, P. He, Z. Wu, A. Amini, N. Wang, C. Cheng, *Adv. Funct. Mater.* **2019**, *29*, 1900527.
[5] K. Pan, W. Wang, E. Shin, K. Freeman, G. Subramanyam, *IEEE Trans. Electron Devices* **2015**, *62*, 2959.
[6] Y. Ke, S. Wang, G. Liu, M. Li, T. J. White, Y. Long, *Small* **2018**, *14*, 1802025.
[7] B. Barazani, G. Dion, J. Morissette, L. Beaudoin, J. Sylvestre, *J. Microelectromech. Syst.* **2020**, *29*, 338.
[8] D. Kalafut, A. Bajaj, A. Raman, *Int. J. Non Linear Mech.* **2020**, *119*, 103304.
[9] G. Gopalakrishnan, D. Ruzmetov, S. Ramanathan, *J. Mater. Sci.* **2009**, *44*, 5345.
[10] S. A. Bukhari, A. Goswami, R. McGee, R. Abraham, D. Hume, H. J. Chung, T. Thundat, presented at *2020 IEEE 33rd International Conference on Micro Electro Mechanical Systems (MEMS)*, IEEE, Vancouver **2020**, pp. 18–22.
[11] a) R. R. Singh, A. Gautam, V. Priye, *Proc. SPIE* **2019**, *10923*, 109231G; b) A. Dash, V. Mere, G. P. Yasasvi, S. Nambiar, A. Naik, S. K. Selvaraja, *Proc. SPIE* **2019**, *10920*, 1092001.
[12] a) D. Kalafut, A. Bajaj, A. Raman, *Int. J. Non-Linear Mech.* **2017**, *95*, 209; b) C. R. Kirkendall, J. W. Kwon, *Sci. Rep.* **2016**, *6*, 22897.
[13] M. Wuttig, H. Bhaskaran, T. Taubner, *Nat. Photonics* **2017**, *11*, 465.
[14] N. F. Mott, L. Friedman, *Philos. Mag.* **1974**, *30*, 389.
[15] R. McGee, A. Goswami, S. Pal, K. Schofield, S. A. M. Bukhari, T. Thundat, *Phys. Rev. Mater.* **2018**, *2*, 034605.
[16] M. F. Jager, C. Ott, P. M. Kraus, C. J. Kaplan, W. Pouse, R. E. Marvel, R. F. Haglund, D. M. Neumark, S. R. Leone, *Proc. Natl. Acad. Sci. USA* **2017**, *114*, 9558.
[17] R. Zhang, Q. S. Fu, C. Y. Yin, C. L. Li, X. H. Chen, G. Y. Qian, C. L. Lu, S. L. Yuan, X. J. Zhao, H. Z. Tao, *Sci. Rep.* **2018**, *8*, 17093.
[18] a) R. McGee, A. Goswami, B. Khorshidi, K. McGuire, K. Schofield, T. Thundat, *Acta Mater.* **2017**, *137*, 12; b) L. L. Fan, Y. F. Wu, C. Si, C. W. Zou, Z. M. Qi, L. B. Li, G. Q. Pan, Z. Y. Wu, *Thin Solid Films* **2012**, *520*, 6124; c) S. Autier-Laurent, B. Mercey, D. Chippaux, P. Limelette, C. Simon, *Phys. Rev. B* **2006**, *74*, 195109.
[19] a) S. Biermann, A. Poteryaev, A. I. Lichtenstein, A. Georges, *Phys. Rev. Lett.* **2005**, *94*, 026404; b) O. Nájera, M. Civelli, V. Dobrosavljević, M. J. Rozenberg, *Phys. Rev. B* **2017**, *95*, 035113.
[20] A. Pergament, A. Velichko, M. Belyaev, V. Putrolaynen, *Physica B* **2018**, *536*, 239.
[21] a) Y. Ke, I. Balin, N. Wang, Q. Lu, A. I. Y. Tok, T. J. White, S. Magdassi, I. Abdulhalim, Y. Long, *ACS Appl. Mater. Interfaces* **2016**, *8*, 33112; b) S. Chen, Z. Wang, H. Ren, Y. Chen, W. Yan, C. Wang, B. Li, J. Jiang, C. Zou, *Sci. Adv.* **2019**, *5*, eaav 6815.
[22] B. M. Younis, A. M. Heikal, M. Hussein, S. S. A. Obayya, M. F. O. Hameed, *Opt. Express* **2019**, *27*, 37454.
[23] Y. Cao, D. Torres, T. Wang, X. Tan, N. Sepúlveda, *Smart Mater. Struct.* **2017**, *26*, 085032.
[24] a) N. Manca, L. Pellegrino, T. Kanki, W. J. Venstra, G. Mattoni, Y. Higuchi, H. Tanaka, A. D. Caviglia, D. Marré, *Adv. Mater.* **2017**, *29*, 1701618; b) T. Wang, D. Torres, F. E. Fernández, C. Wang, N. Sepúlveda, *Sci. Adv.* **2019**, *3*; c) C. Huang, Z. Zhang, S. Ramanathan, D. Weinstein, *IEEE Trans. Electron Devices* **2019**, *66*, 4380.
[25] R. E. Simpson, P. Fons, A. V. Kolobov, T. Fukaya, M. Krbal, T. Yagi, J. Tominaga, *Nat. Nanotechnol.* **2011**, *6*, 501.
[26] T. Cao, R. E. Simpson, M. J. Cryan, *J. Opt. Soc. Am. B* **2013**, *30*, 439.
[27] L. Mao, Y. Li, G. Li, S. Zhang, T. Cao, *Adv. Photonics* **2020**, *2*, 056004.
[28] a) P. Parikh, C. Chakraborty, T. S. Abhilash, S. Sengupta, C. Cheng, J. Wu, M. M. Deshmukh, *Nano Lett.* **2013**, *13*, 4685; b) S. Sengupta, K. Wang, K. Liu, A. K. Bhat, S. Dhara, J. Wu, M. M. Deshmukh, *Appl. Phys. Lett.* **2011**, *99*, 062114.
[29] G. Seo, B.-J. Kim, Y. W. Lee, H.-T. Kim, *Appl. Phys. Lett.* **2012**, *100*, 011908.
[30] M. Reina, R. Messina, S.-A. Biehs, P. Ben-Abdallah, *Phys. Rev. B* **2020**, *101*, 041409.
[31] Y. Cao, N. Sepúlveda, *Adv. Mater. Interfaces* **2019**, *6*, 1900887.
[32] a) N. Manca, L. Pellegrino, T. Kanki, S. Yamasaki, H. Tanaka, A. S. Siri, D. Marré, *Adv. Mater.* **2013**, *25*, 6430; b) L. Pellegrino, N. Manca, T. Kanki, H. Tanaka, M. Biasotti, E. Bellingeri, A. S. Siri, D. Marré, *Adv. Mater.* **2012**, *24*, 2929; c) Y. Jung, J. Jeong, Z. Qu, B. Cui, A. Khanda, S. S. P. Parkin, J. K. S. Poon, *Adv. Electron. Mater.* **2021**, *7*, 2001142.
[33] M. Nakajima, N. Takubo, Z. Hiroi, Y. Ueda, T. Suemoto, *Appl. Phys. Lett.* **2008**, *92*, 011907.
[34] H. T. Stinson, A. Sternbach, O. Najera, R. Jing, A. S. McLeod, T. V. Slusar, A. Mueller, L. Anderegg, H. T. Kim, M. Rozenberg, D. N. Basov, *Nat. Commun.* **2018**, *9*, 3604.
[35] N. Shukla, A. Parihar, E. Freeman, H. Paik, G. Stone, V. Narayanan, H. Wen, Z. Cai, V. Gopalan, R. Engel-Herbert, D. G. Schlom, A. Raychowdhury, S. Datta, *Sci. Rep.* **2014**, *4*, 4964.
[36] a) M. N. Sadiq, M. L. Roy, A. Perennec, P. Laurent, N. Martin, D. Passerieux, A. Crunteanu, R. Boyer, F. Dumas-Bouchiat, M. B. Martin, L. Divay, Q. Levesque, G. Tanné, presented at *2019 IEEE MTT-S International Microwave Workshop Series on Advanced Materials and Processes for RF and THz Applications (IMWS-AMP)*, Vol. *16–18*, IEEE, Los Angeles , CA **2019**, p. 2019; b) A. Cavalleri, C. Tóth, C. W. Siders, J. A. Squier, F. Ráksi, P. Forget, J. C. Kieffer, *Phys. Rev. Lett.* **2001**, *87*, 237401.
[37] M. J. Avedillo, J. M. Quintana, J. Núñez, *IEEE Trans. Nanotechnol.* **2020**, *19*, 107.
[38] D. Bhardwaj, A. Goswami, A. M. Umarji, *J. Appl. Phys.* **2018**, *124*, 135301.
[39] S. A. Bukhari, S. Kumar, P. Kumar, S. P. Gumfekar, H.-J. Chung, T. Thundat, A. Goswami, *Appl. Surf. Sci.* **2020**, *529*, 146995.
[40] W.-M. Zhang, K.-M. Hu, Z.-K. Peng, G. Meng, *Sensors* **2015**, *15*, 26478.
[41] R. McGee, A. Goswami, R. Abraham, S. Bukhari, T. Thundat, *MRS Adv.* **2018**, *3*, 359.
[42] R. McGee, A. Goswami, S. A. M. Bukhari, L. Zhou, K. Shankar, T. Thundat, *J. Microelectromech. Syst.* **2019**, *28*, 766.
[43] T. V. Son, V. V. Truong, J.-F. Bisson, A. Haché, *Appl. Phys. Lett.* **2017**, *111*, 041103.
[44] N. Wang, S. Liu, X. T. Zeng, S. Magdassi, Y. Long, *J. Mater. Chem. C* **2015**, *3*, 6771.
[45] E. Breckenfeld, H. Kim, E. P. Gorzkowski, T. E. Sutto, A. Piqué, *Appl. Surf. Sci.* **2017**, *397*, 152.
[46] S. Lee, K. Hippalgaonkar, F. Yang, J. Hong, C. Ko, J. Suh, K. Liu, K. Wang, J. J. Urban, X. Zhang, C. Dames, S. A. Hartnoll, O. Delaire, J. Wu, *Science* **2017**, *355*, 371.
[47] R. Basu, P. Magudapathy, M. Sardar, R. Pandian, S. Dhara, *J. Phys. D: Appl. Phys.* **2017**, *50*, 465602.
[48] J.-H. Yu, S.-H. Nam, J. W. Lee, J.-H. Boo, *Materials* **2016**, *9*, 556.
[49] D. Systèmes, Abaqus 6.13 Abaqus/CAE User's Guide, **2013**.

